SmartScope: Framework for Autonomous Cryo-EM Imaging

Jonathan Bouvette[1], Qinwen Huang[2], Amanda A. Riccio[1], William C. Copeland[1], Alberto Bartesaghi[2,3,4*] and Mario J. Borgnia[1*]

[1] Genome Integrity and Structural Biology Laboratory, National Institute of Environmental Health Sciences, National Institutes of Health, Department of Health and Human Services, Research Triangle Park, NC, USA.
[2] Department of Computer Science, Duke University, Durham, NC, USA.
[3] Department of Biochemistry, Duke University, Durham, NC, USA.
[4] Department of Electrical and Computer Engineering, Duke University, Durham, NC, USA.
[*] Co-corresponding authors: mario.borgnia2@nih.gov, alberto.bartesaghi@duke.edu

SmartScope is a framework for automated evaluation and imaging of cryo-electron microscopy (cryo-EM) specimens. It can learn from expert annotations on past experiments and refine its underlying AI to improve the selection of biologically relevant targets. Through its intuitive web interface, SmartScope assists users in exploring specimens and optimizing the outcome of each experiment, ultimately lowering the barriers to the adoption of cryo-EM.

Optimal specimens are critical in structure determination by cryo-EM. The ideal specimen is a single layer of macromolecular complexes embedded into a thin slab of vitrified buffer. Macromolecules are thus confined between hydrophobic interfaces with air and substrates, which can lead to denaturation and aggregation. In addition, current vitrification methods typically yield variations in ice thickness across the grid. During optimization, several parameters are varied iteratively to improve the stability and mono-dispersity of the target, and the uniformity of the ice layer. Changes include purification protocols, chemical additives, support material and freezing conditions [1]. Each combination is subjected to comprehensive sampling using a cryo-electron microscope. This lengthy evaluation provides critical information for subsequent iterations but constitutes a rate limiting step in structure determination by cryo-EM.

Manual specimen screening involves selecting area, adjusting the optical conditions of the microscope, and recording images. This requires attention to repetitive tasks and careful bookkeeping. The subjectivity in the selection of areas can lead to suboptimal sampling. Consequently, the quality of the process depends on skilled microscopists. SmartScope addresses these shortcomings by automating and optimizing how imaging experiments are conducted, thus significantly reducing the workload, and making cryo-EM accessible to non-specialists (Fig. 1A).

SmartScope uses the SerialEM [2] API to automate all microscope operations necessary to navigate the specimen enabling autonomous exploration of specimens (Fig. 1A). Results are displayed through a secure web interface that allows modification of automatically selected targets in real time, effectively enabling remote operation of the microscope. Micrographs and metadata are stored in a consistent data structure preserving spatial relationships between images to ensure adequate record keeping. The web interface doubles as a portal to the database to facilitate off-line evaluation of the results.

Once a specimen is loaded for imaging, a low-magnification map (atlas) of the grid is acquired. Areas suitable for imaging appear as "windows", commonly squares [4], through the grid in which the support layer is intact and not blocked by thick ice or large contaminants. Windows are automatically detected and classified using a pretrained Region-based Convolutional Neural Network [5] that identifies the "good" windows with 80% precision, efficiently guiding the instrument to desirable regions of the grid. (Fig 2A). A user-specified number of these windows selected based on size to maximize sampling diversity is imaged at a higher magnification to identify regions of interest. In this study, we implemented a robust method for hole detection for single-particle cryo-EM specimens based on the You-Only-Look-Once [6] object detection architecture (Fig. 2B). A classification step excludes contaminants, allowing for correct identification of 89% of the holes. After detection, a subset of holes is selected based on their relative pixel intensity. The robustness of these feature recognition algorithms allows complete automation of the screening process.

In screening mode, the median sampling time for a specimen is 21 min, yielding a median of 9.0 high-magnification images sampled from 3.0 different windows (Fig. 1B). Daily, our microscope screens 16 specimens and perform data collecting for approximately 16 hours.

In data collection mode, the microscope continuously acquires areas and finds targets using operator assistance to tune the selection to specific needs, reducing setup time to 32 min using a K2 detector. An algorithm was designed to group targets for beam-image shift (BIS) acquisition within a given radius while minimizing the number of stage movements and maximizing coverage. It also supports BIS data collection on tilted specimens by correcting coordinates and defocus based on tilt constraints (Fig. 1C) [7]. As an example, we used SmartScope to determine a 3.4 Å map of the 110 kDa POLG2 [8] (Fig. 3).

SmartScope can fully automate the cryo-EM screening workflow and perform non-stop data acquisition facilitating data collection setup, and making the most out of each imaging session. The ability to change collection parameters on-the-fly opens the possibility of integrating feedback from in-line data processing workflows to adaptively improve image quality during acquisition. Most cryo-EM facilities collaborate with external users via remote desktop access to the instruments [9]. SmartScope offers a convenient web-based alternative where multiple users can simultaneously access their session. Unsupervised multi-specimen screening and short exploratory data collection sessions can be scheduled to run overnight, maximizing microscope usage. The software platform was designed to easily incorporate additional selection criteria [10–14] and workflows as plugins. The client-server architecture of SmartScope combined with its AI-driven feature detection engine, offers the possibility of envisioning a "virtual microscopist" that could constantly improve its capabilities through periodic re-training based on voluntary submission of curated datasets.
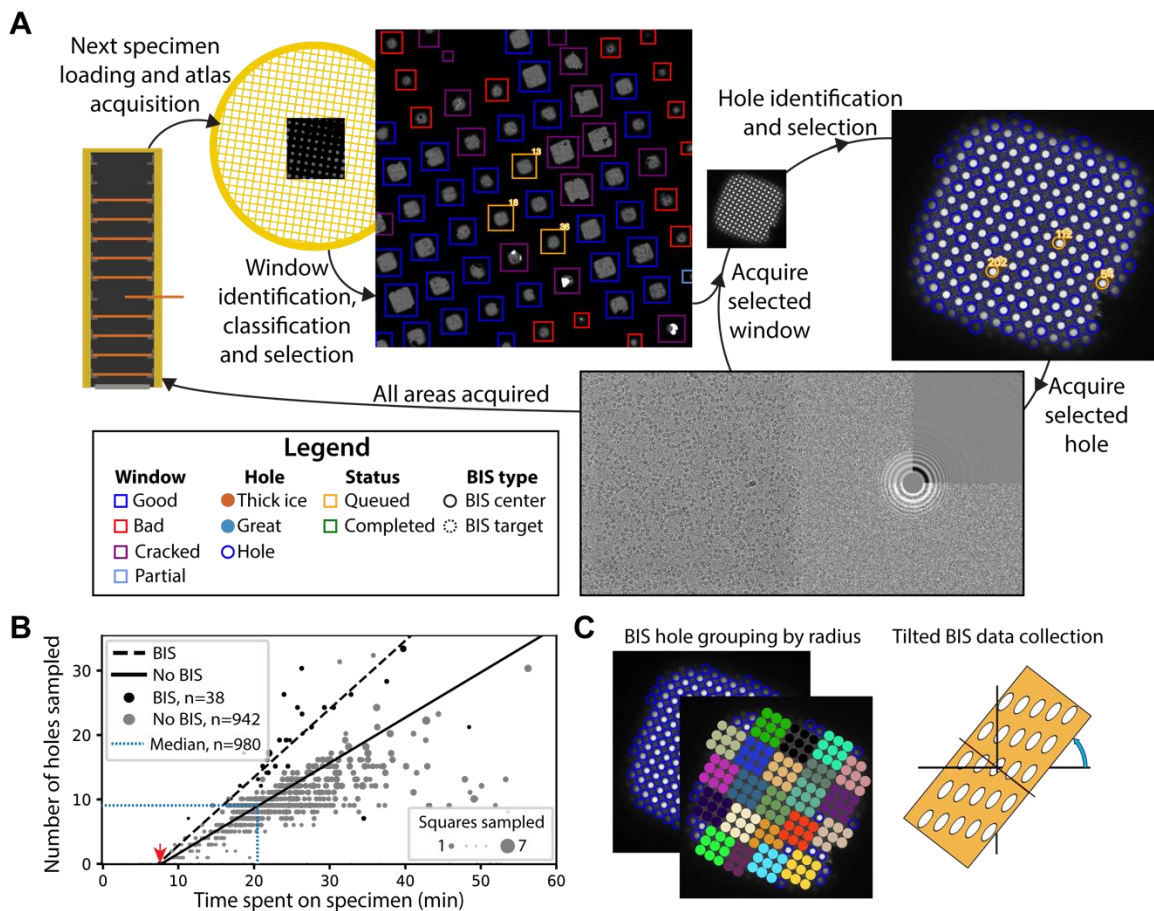
The source code will be available at https://gitlab.cs.duke.edu/bartesaghilab/smartscope.

Figure 1. Overview of the SmartScope framework. **A** Workflow for autonomous grid navigation and imaging. SmartScope handles specimen exchange, atlas acquisition, window identification, classification, and selection. It then visits the selected areas and identifies and selects holes which are acquired at higher magnification and preprocessed. **B** Screening mode statistics. Screening rates without and with BIS were 0.7 and 1.0 holes per minute respectively (RANSAC regression). The red arrow indicates specimen loading and atlas acquisition overhead time. **C** Example of the BIS hole grouping (left) and tilted acquisition with focus and coordinate correction based on tilt constraints (right).
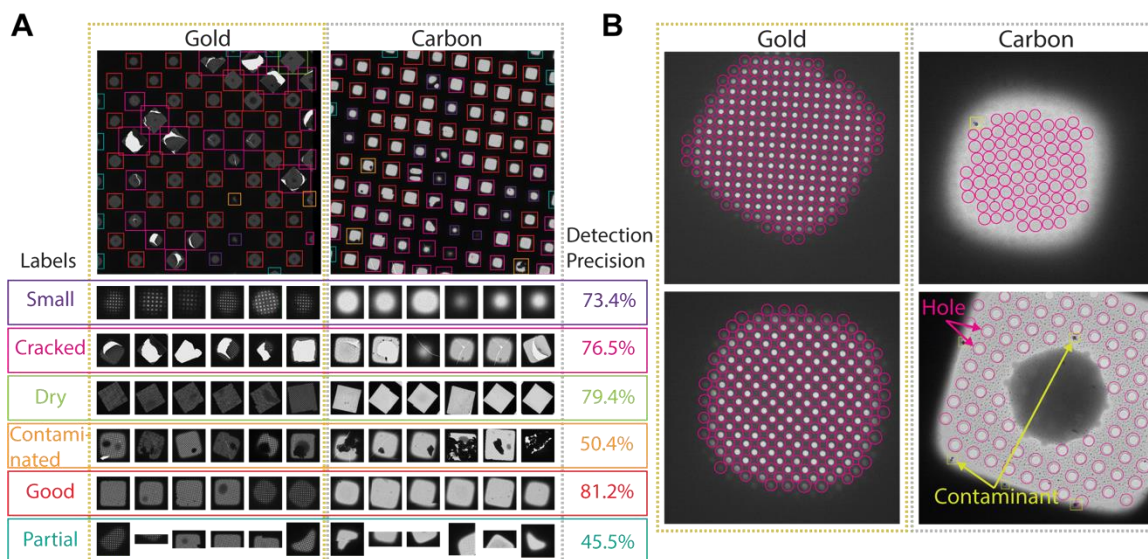
Figure 2. Deep-learning based feature recognition for autonomous navigation. Inference phases of the window (**A**) and hole classifiers (**B**) applied to carbon and gold grids. Image sets were annotated manually, subjected to data augmentation, and used for training. These models are then used for real-time object detection and classification.
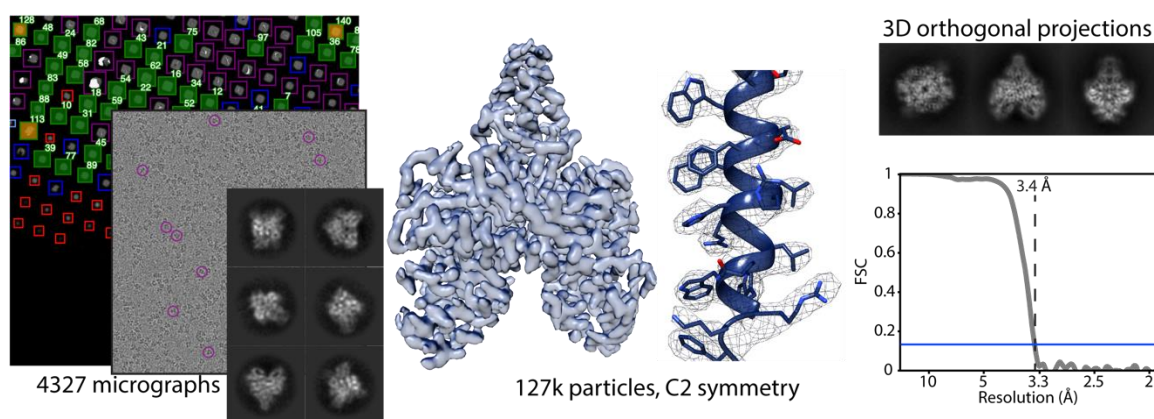

Figure 3. Acquisition of POLG2 dataset using SmartScope and data processing to 3.4Å resolution.

References:

[1] L. A. Passmore, C. J. Russo, In Methods in Enzymology (Ed.: Crowther, R. A.), Academic Press, (2016), pp. 51–86.
[2] D. N. Mastronarde, J. Struct. Biol. (2005), **152**, 36.
[3] C. Suloway, J. Pulokas, D. Fellmann, A. Cheng, F. Guerra, J. Quispe, S. Stagg, C. S. Potter, B. Carragher, J. Struct. Biol. (2005), **151**, 41.
[4] K. Naydenova, P. Jia, C. J. Russo, Science (2020), **370**, 223.
[5] R. Girshick, ArXiv150408083 Cs (2015).
[6] J. Redmon, S. Divvala, R. Girshick, A. Farhadi, ArXiv150602640 Cs (2016).
[7] J. Bouvette, H.-F. Liu, X. Du, Y. Zhou, A. P. Sikkema, J. da Fonseca Rezende e Mello, B. P. Klemm, R. Huang, R. M. Schaaper, M. J. Borgnia, A. Bartesaghi, Nat. Commun. (2021), **12**, 1957.

[8] M. J. Young, W. C. Copeland, In Mitochondrial Disorders Caused by Nuclear Genes (Ed.: Wong, L.-J. C.), Springer, New York, NY, (2013), pp. 49–72.

[9] B. Alewijnse, A. W. Ashton, M. G. Chambers, S. Chen, A. Cheng, M. Ebrahim, E. T. Eng, W. J. H. Hagen, A. J. Koster, C. S. López, N. Lukoyanova, J. Ortega, L. Renault, S. Reyntjens, W. J. Rice, G. Scapin, R. Schrijver, A. Siebert, S. M. Stagg, V. Grum-Tokars, E. R. Wright, S. Wu, Z. Yu, Z. H. Zhou, B. Carragher, C. S. Potter, J. Struct. Biol. (2017), **199**, 225.

[10] M. Schorb, I. Haberbosch, W. J. H. Hagen, Y. Schwab, D. N. Mastronarde, Nat. Methods (2019), **16**, 471.

[11] H. Xu, D. E. Timm, S. Y. Elhabian, In Medical Image Computing and Computer Assisted Intervention – MICCAI 2020 (Eds.: Martel, A. L.; Abolmaesumi, P.; Stoyanov, D.; Mateus, D.; Zuluaga, M. A.; Zhou, S. K.; Racoceanu, D.; Joskowicz, L.), Springer International Publishing, Cham, (2020), pp. 56–65.

[12] Y. Yokoyama, T. Terada, K. Shimizu, K. Nishikawa, D. Kozai, A. Shimada, A. Mizoguchi, Y. Fujiyoshi, K. Tani, Biophys. Rev. (2020), **12**, 349.

[13] K. Yonekura, S. Maki-Yonekura, H. Naitow, T. Hamaguchi, K. Takaba, Commun. Biol. (2021), **4**, 1.

[14] P. T. Kim, A. J. Noble, A. Cheng, T. Bepler, ArXiv211201534 Cs Eess Q-Bio (2021).

[15] These authors contributed equally: Jonathan Bouvette, Qinwen Huang.